JOURNAL OF SPACECRAFT AND ROCKETS
Vol. 46, No. 2, March–April 2009

Heating Augmentation for Short Hypersonic Protuberances

Alireza Mazaheri*
Analytical Mechanics Associates, Inc., Hampton, Virginia 23666
NASA Langley Research Center, Hampton Virginia 23681
and
William A. Wood†
NASA Langley Research Center, Hampton Virginia 23681

DOI: 10.2514/1.39992

Computational aeroheating analyses of the Space Shuttle Orbiter plug-repair models are validated against data collected in the Calspan—University of Buffalo Research Center 48 in. shock tunnel. The comparison shows that the average difference between computed heat transfer results and the data is about 9.5%. Using computational fluid dynamics and wind-tunnel data, an empirical correlation for estimating heating augmentation on short hypersonic protuberances ($k/\delta < 0.3$) is proposed. This proposed correlation is compared with several computed flight simulation cases and good agreement is achieved. Accordingly, this correlation is proposed for further investigation on other short hypersonic protuberances for estimating heating augmentation.

Nomenclature

C_p	=	specific heat, BTU/slugs · R
d	=	plug-repair diameter, in.
k	=	protuberance height, in.
M	=	Mach number
p	=	pressure, lb/ft^2
q	=	heat transfer rate, BTU/ft^2 · s
Re	=	unit Reynolds number, 1/ft
r	=	constant
St	=	Stanton number
T	=	temperature, R
V	=	total velocity, ft/s
x, y, z	=	coordinate system, in.
α	=	angle of attack, deg
δ	=	boundary-layer thickness, in.
δ^*	=	displacement thickness, in.
ϵ	=	emissivity
θ	=	momentum thickness, in.
μ	=	viscosity, lb · s/ft^2
ρ	=	density, slugs/ft^3

Subscripts

i, j, k	=	grid-point indices
p	=	plug repair
rf	=	recovery factor
t	=	total
w	=	wall
x, y, z	=	local x, y, and z coordinates
θ	=	momentum thickness
$\langle\cdot\rangle$	=	average value
∞	=	freestream

Presented as Paper 4255 at the 40th AIAA Thermophysics Conference, Seattle, WA, 23–26 June 2008; received 23 July 2008; revision received 12 October 2008; accepted for publication 17 October 2008.

*Aerothermodynamics Branch; Ali.R.Mazaheri@nasa.gov. Member AIAA.
†Aerothermodynamics Branch; William.A.Wood@nasa.gov. Senior Lifetime Member AIAA.

Introduction

FOLLOWING the Space Shuttle *Columbia* accident in 2003, NASA investigated methods for performing on-orbit repairs to the thermal protection system and their impacts on the aerothermodynamic environment of the Space Shuttle Orbiter experienced during reentry [1]. Various methods were developed to repair damaged areas of the Space Shuttle Orbiter, including the use of tile repairs and plug repairs that are used on orbit to patch small breaches on the orbiter tile and on the wing leading-edge (WLE) reinforced carbon–carbon panels, respectively. Several studies have been reported for the aeroheating analysis of the tile and plug repairs (see [2–7]). However, no correlation has been reported to estimate the augmented maximum heating that results from disturbing the local flowfield.

The aim of this investigation is to obtain a heating-augmentation correlation for a hypersonic repair surface using flowfield information around the smooth outer mold line (OML) of the vehicle. The focus of this study is on the Space Shuttle Orbiter. Aerothermodynamic computations are studied for wind-tunnel swept-cylinder models with rounded protuberances of different heights placed on the cylinder. Computational fluid dynamics (CFD) simulations are obtained for the wind-tunnel (WT) cases, and the

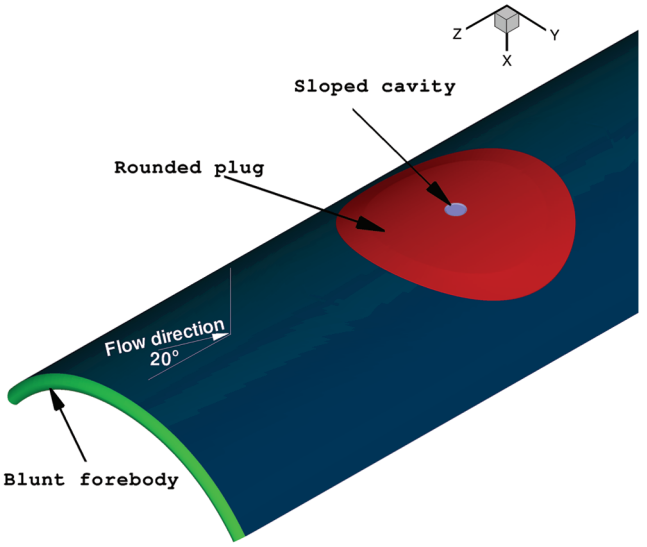

Fig. 1 Schematic of the wind-tunnel model.

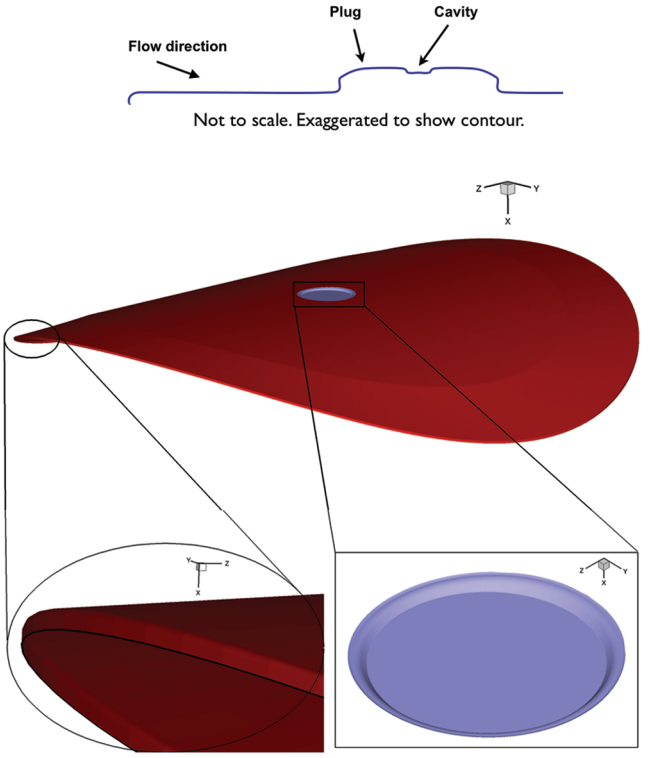

Fig. 2 Schematic of the plug shape with its cavity.

results are compared with the WT data. Based on CFD and WT data, a simple heating-augmentation correlation is proposed for comparison with several flight CFD data. The correlation does require that shuttle smooth-OML results are available.

CFD Validation

In this section, computational analyses are validated against available wind-tunnel data. The validation is necessary to extrapolate the CFD data to flight conditions for which a heating-augmentation correlation is needed.

Computational Procedures

Computational aerothermodynamic analyses are conducted using LAURA [8,9], which is a chemically reacting viscous flow solver. Computations are performed for three-dimensional swept-cylinder models, which are shown schematically in Figs. 1 and 2.

Several different plug heights are considered. The plug dimensions and wind-tunnel flow conditions corresponding to the experimental run numbers are given in Table 1. Perfect-gas air is used during the experiments. Experiments are conducted by Calspan—University of Buffalo Research Center [10] in a 48 in. shock tunnel. Computations are simulated at the wind-tunnel conditions with a perfect-gas-air model.

Because each WT model was individually manufactured, a specific grid was needed for each of the models to account for their

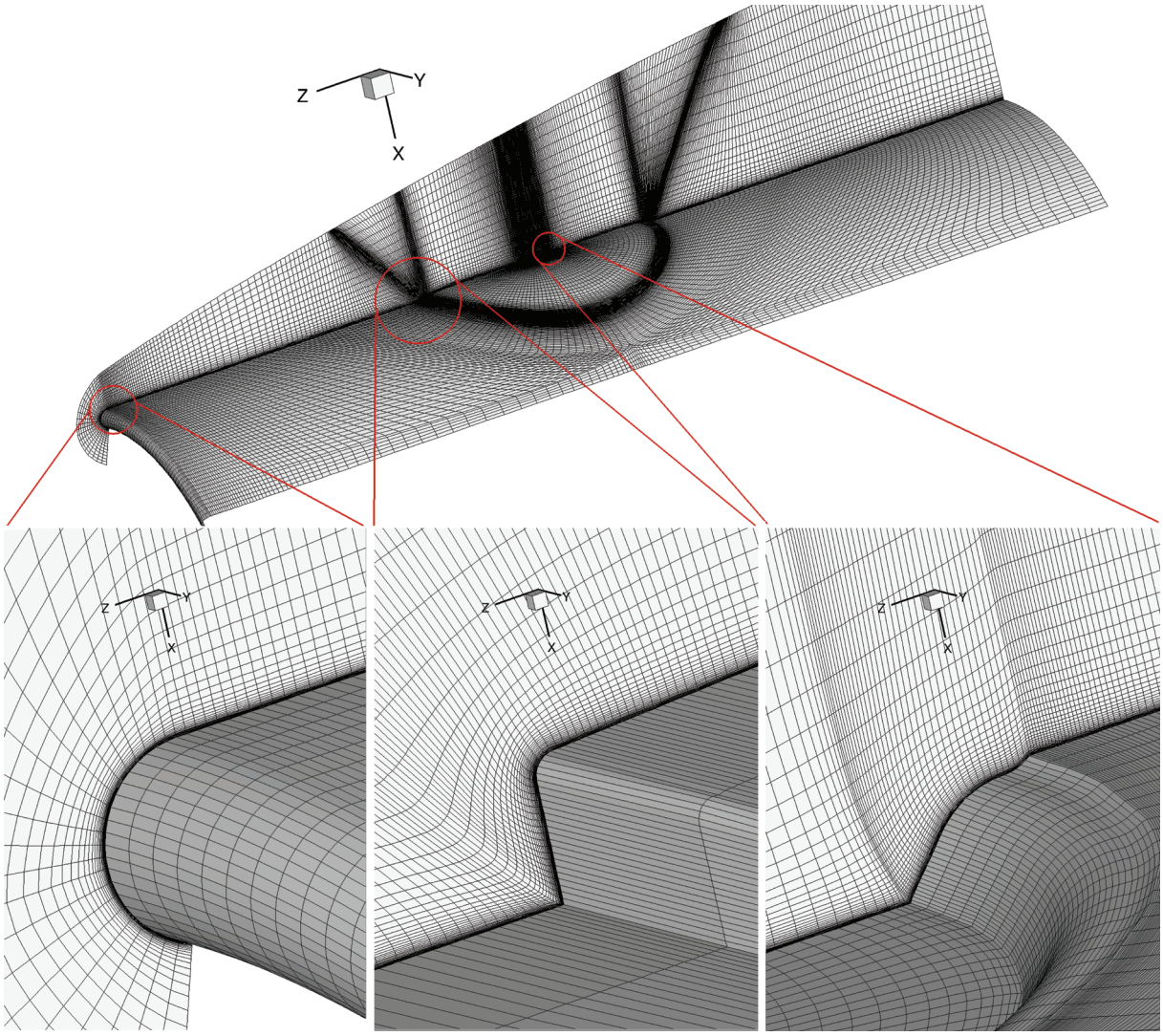

Fig. 3 Viscous grid developed for a wind-tunnel swept-cylinder model.

Table 1 Plug dimensions and wind-tunnel flow conditions corresponding to the experimental run numbers

Run number	d_p, in.	k_p, in.	M_∞	V_∞, ft/s	$\rho_\infty \times 10^6$, slugs/ft^3	T_∞, R	$Re \times 10^{-6}$, 1/ft	k/δ
15	7	0.025	11.60	6290	2.86	122	0.19	0.11
13	7	0.045	11.57	6360	2.80	126	0.18	0.20
28	7	0.055	11.68	6270	2.77	120	0.19	0.24
11	7	0.065	11.68	6190	2.77	117	0.19	0.28

Table 2 Parameters used in the Stanton number calculations

k_p, in.	C_p, BTU/slugs · R	T_w, R	T_t, R
0.025	7.7247	526	3110
0.045	7.7081	526	3170
0.055	7.7286	521	3090
0.065	7.7519	525	3020

precise features. A grid topology was designed to generate smooth grids that can capture geometrical features of the model and physical behavior of hypersonic flow around the body. A schematic of the developed viscous grid is shown in Fig. 3. More details of the grid-generating techniques are reported in [11].

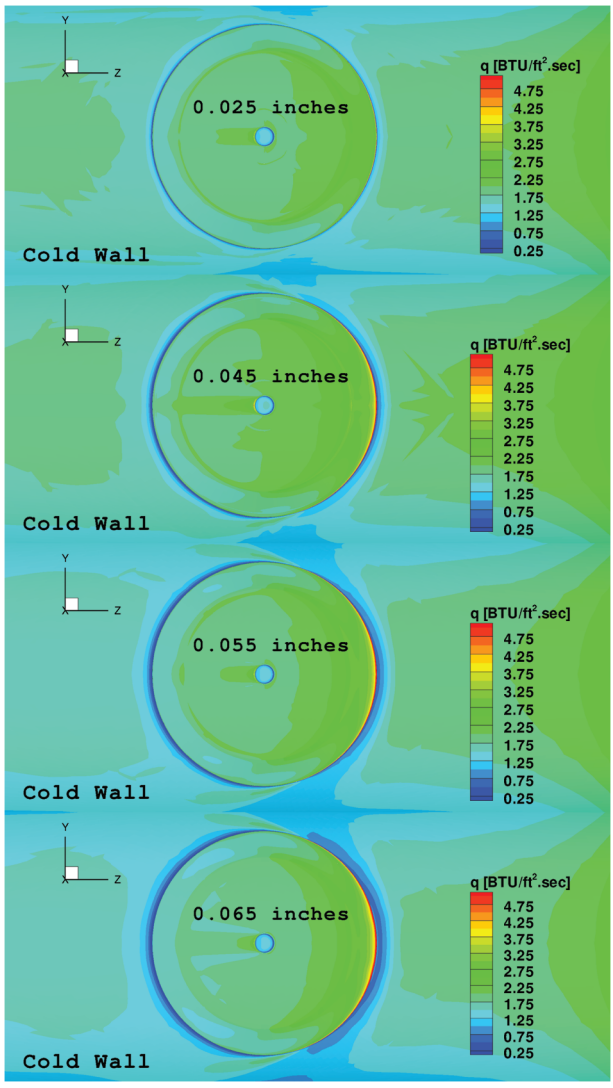

Fig. 4 Computed surface heat flux variations on the plug area of the wind-tunnel geometries. Flow direction is from right to left.

Table 3 Differences between computed and measured surface heat flux

	Error %				
Data point	0.025 in.	0.045 in.	0.055 in.	0.065 in.	⟨|error|⟩, %
1	−2.7	+3.0	−1.5	−5.2	3.1
2	−6.8	+13.2	+8.53	+4.4	8.2
3	+17.5	−0.6	+12.4	−12.6	10.8
4	+11.5	+5.9	−10.2	−19.3	11.7
5	+16.9	+1.9	+4.3	−12.8	9.0
6	+13.0	+4.7	+13.0	−2.5	8.3
7	−58.6	+21.0	+34.0	+9.2	30.7
8	−11.8	+24.3	−3.7	−1.6	10.3
9	−11.6	+19.2	+5.6	+7.0	10.8
10	−5.4	+18.9	+11.9	+10.9	11.8
11	+3.3	+19.6	+1.9	−6.5	7.8
12	+0.7	+8.4	+12.0	+3.3	6.1
13	−10.2	+2.4	+13.1	+0.2	6.5
14	−13.1	——	−3.4	−8.1	8.2
15	+4.8	13.2	+7.3	+0.8	6.5
16	−11.3	+4.9	+0.4	−6.8	5.9
17	−3.6	+6.4	+6.7	+3.8	5.1

Table 4 Distance from the base of the plug to a location at which the peak heating is measured by gauge 8

Plug height, in.	η, in.
0.025	0.0223
0.045	0.0423
0.055	0.0523
0.065	0.0623

Computational Results

Wind-tunnel models, each consisting of a 7 in. rounded plug on a swept cylinder with a blunted nose, shown in Figs. 1 and 2, are analyzed at the wind-tunnel conditions given in Table 1. As stated before, perfect-gas air is used for both wind-tunnel experiments and computations. Simulations are conducted with the WT conditions for which the surface temperatures are relatively constant (cold wall). WT conditions are assumed to be laminar, as laminar flow was reported [12] for a series of experiments conducted at the same facility on a different model with Mach 10 (relatively the same Mach number as in the present study), $\alpha = 40$, and $Re = 2.41 \times 10^6$ 1/ft (more than 12 times the Reynolds number reported here). Therefore, only laminar flow is computed.

Contour plots of the computed surface heat fluxes are shown in Fig. 4. This figure shows that the plug surface heat flux increases with the plug height. The local surface heat flux is employed and local surface Stanton number is calculated.

The main goal of this study is to obtain a correlation that may be used for flight conditions in which the surface is at radiative equilibrium, with surface emissivity of $\epsilon = 0.89$. Consequently, the Stanton number is obtained for radiative equilibrium surface conditions. The Stanton number is calculated as

$$St = q_w/(\rho_\infty V_\infty C_p(r_{\text{rf}} T_t - T_w)) \tag{1}$$

where q_w is surface heat flux, ρ_∞ is freestream density, V_∞ is

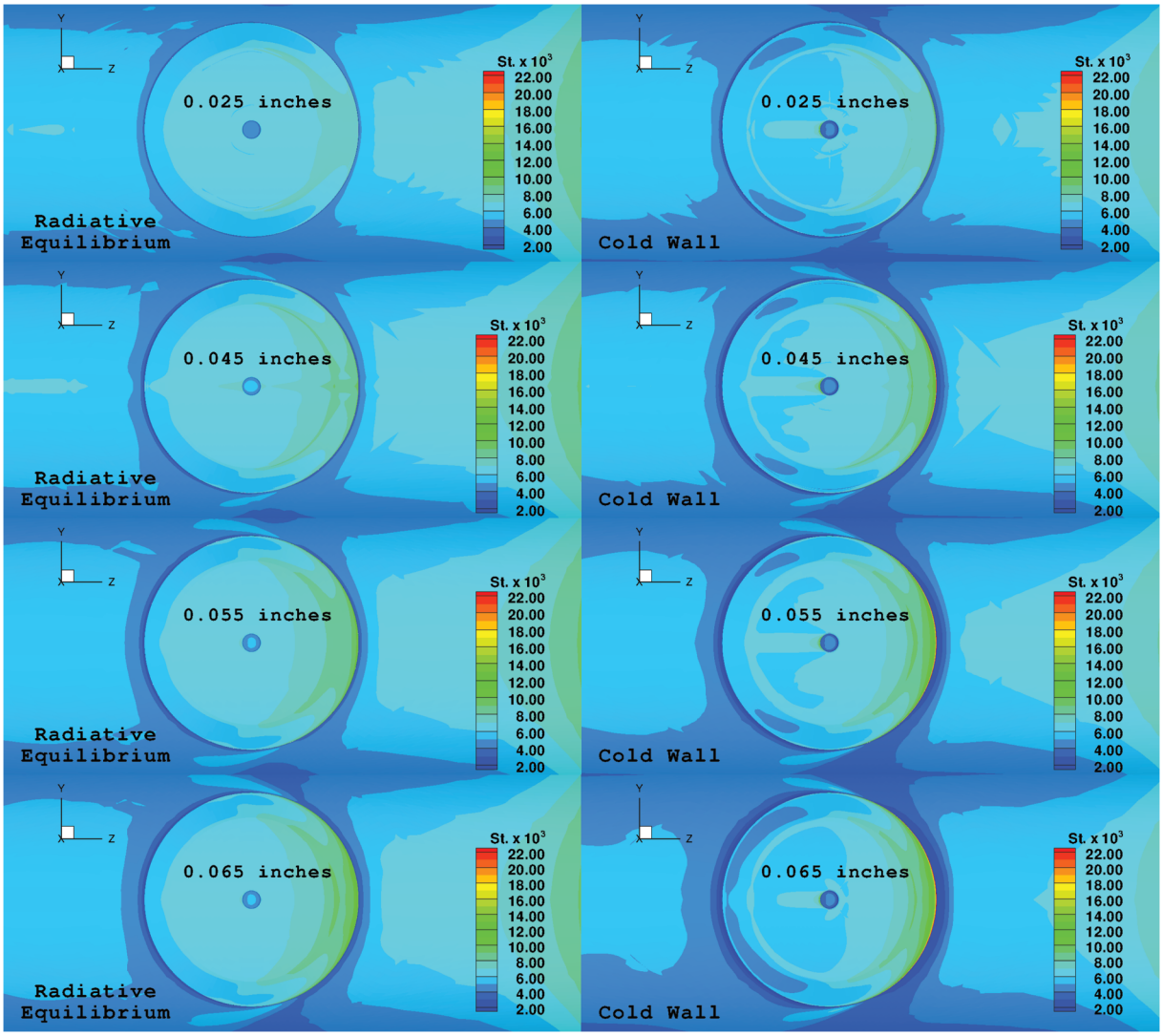

Fig. 5 Stanton number variations on the plug area of the wind-tunnel geometries. Flow direction is from right to left.

freestream velocity, C_p is specific heat at constant pressure, r_{rf} is a constant recovery factor, T_t is total temperature, and T_w is surface temperature. The values of freestream density and velocity are given in Table 1, and values of specific heat, total temperature, and wall temperature are given in Table 2. A constant recovery factor of 0.92 is used for all of the calculations.[‡] The surface Stanton number variations are plotted in Fig. 5.

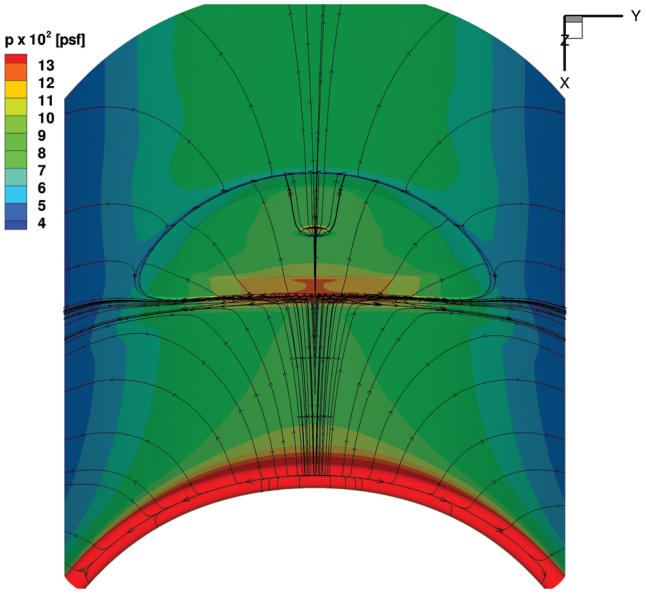

Fig. 6 Stream traces of flow around the 0.065 in. wind-tunnel geometry.

Specific-heat values are calculated based on wind-tunnel conditions. For the radiative equilibrium wall condition, local surface temperature is used. Figure 5 shows that the local Stanton number computed with the radiative equilibrium wall-temperature boundary condition does not entirely match that computed with the cold-wall boundary condition. The difference is largest at the plug leading edge and becomes comparable far upstream and downstream of the plug.

For all WT cases, the flow spreads to both sides of the plug before passing the plug leading edge and causing a small recirculation region upstream of the plug. Streamlines on the plug's top surface are similar, with a recirculation zone just downstream of the cavity trailing edge. These flow features are schematically shown in Fig. 6 for the 0.065 in. plug.

Computational Validation

The CFD analyses are validated by comparing the numerical data with the WT data. The surface heat flux probe locations are shown in Fig. 7. Table 3 summarizes the differences in computational and experimental [10] surface heat flux data for all gauge locations. The averages of absolute percentage errors are also given in the last column. This table shows that the averaged data from the CFD

[‡]Private communication with B. Anderson of NASA Johnson Space Center, 2007.

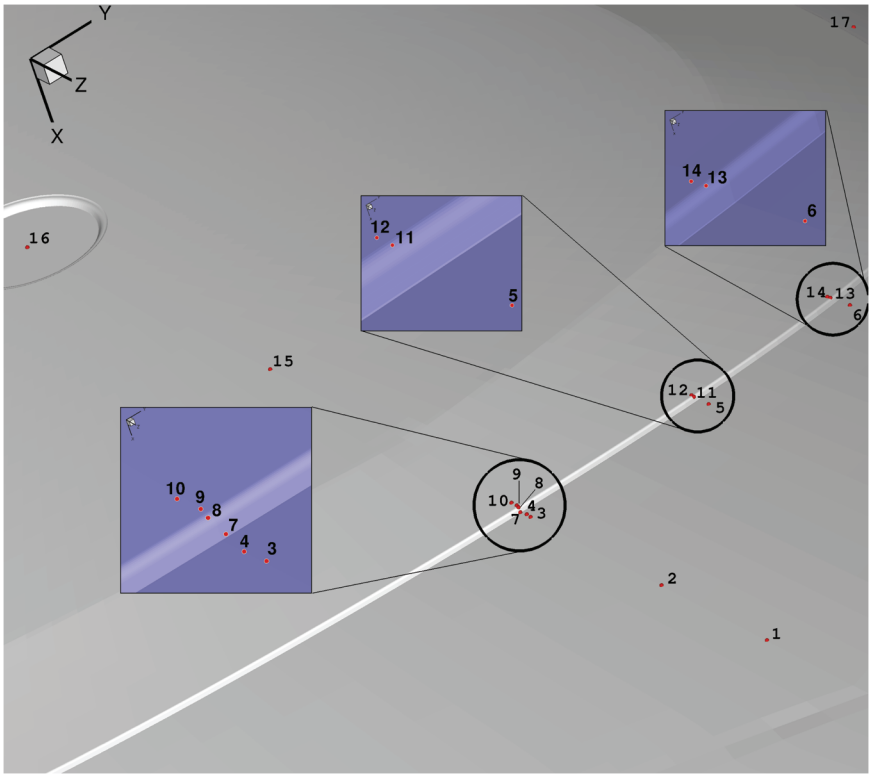

Fig. 7 Surface data points.

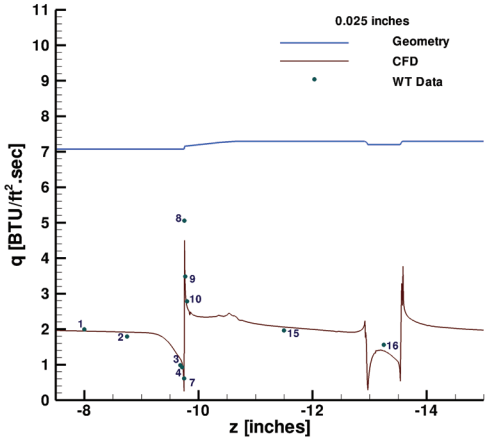

a) 0.025 inch plug

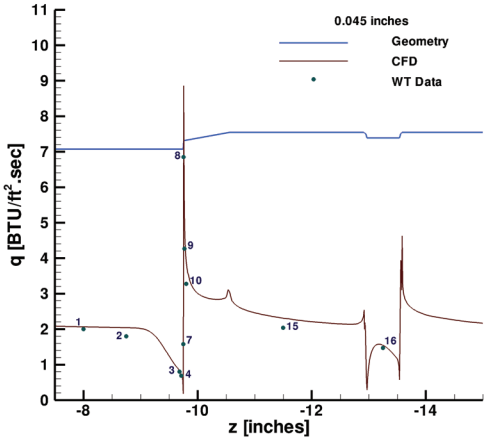

b) 0.045 inch plug

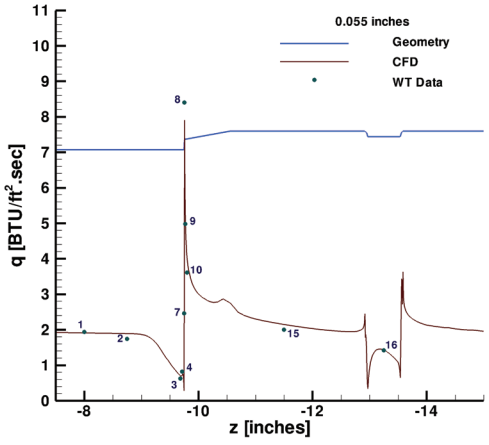

c) 0.055 inch plug

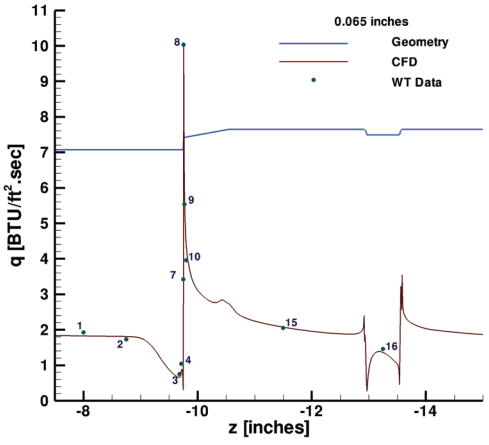

d) 0.065 inch plug

Fig. 8 Heat flux variations along the WT geometry.

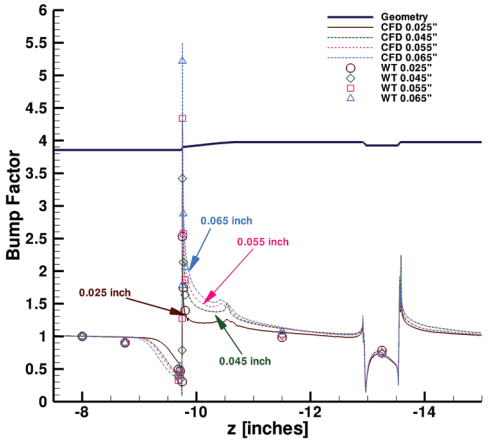

Fig. 9 Heating BF along the WT geometry.

simulation are within 12% of the experimental data, except for probe 7, for which the average difference is about 30%. Probe 7 is located at the base of the plug, where it meets the swept cylinder, and a large error is possibly due to geometrical modeling limitation in such an area. Because of the orthogonality of these areas with respect to the swept cylinder and the fact that all of the grid lines normal to the surfaces must be brought to the outer boundary to effectively align the grid lines with the bow shock during the simulation, these areas experience insufficient grid resolutions. The average difference between computed and reported WT heat transfer data is about 8 and 9.5%, with and without considering probe 7, respectively.

The accuracy of the numerical results is emphasized in Fig. 8 by showing heat flux variations with distance along a line that connects the two probe points 1 and 16 (see Fig. 7). Wind-tunnel data are also shown in this figure with plug geometry variations. A very good agreement with WT data is achieved, with a maximum average difference of 12%, except for probe 7, for which the maximum average difference is about 30%, which is explained as geometrical modeling limitations. This figure shows that the peak heating increases with the plug height.

To compare heat fluxes on the WT model plug with different heights, the surface heat flux of each model is normalized by the local heat flux at probe location 1. This states the heating bump factor (BF). The results are plotted in Fig. 9. The experimental BF data are also shown in this figure. As shown, the BF on the plug top surface increases with plug height.

To quantify the CFD accuracy, computed heat fluxes at gauge locations 1–10 (see Fig. 7) are plotted with the measured WT data in Fig. 10, in which a good agreement is shown. In this figure, the WT errors are the repeatability errors. This figure shows that the highest surface heat flux on the plug for all of the cases occurs at gauge 8. The difference between the highest computed and measured heat flux is within 5% for all of the cases except for the 0.045 in. case, in which it is 20%. As a result of the good comparisons, these data are employed to develop a generalized heating-augmentation correlation that simplifies the prediction process. The intent is then to demonstrate the analysis can be formulated to flight conditions and can be used for flight analysis. This is described in the next section.

Heating Augmentation Correlation

The computational results and the WT data are used to develop a heating-augmentation (HA) correlation for plug repair at flight

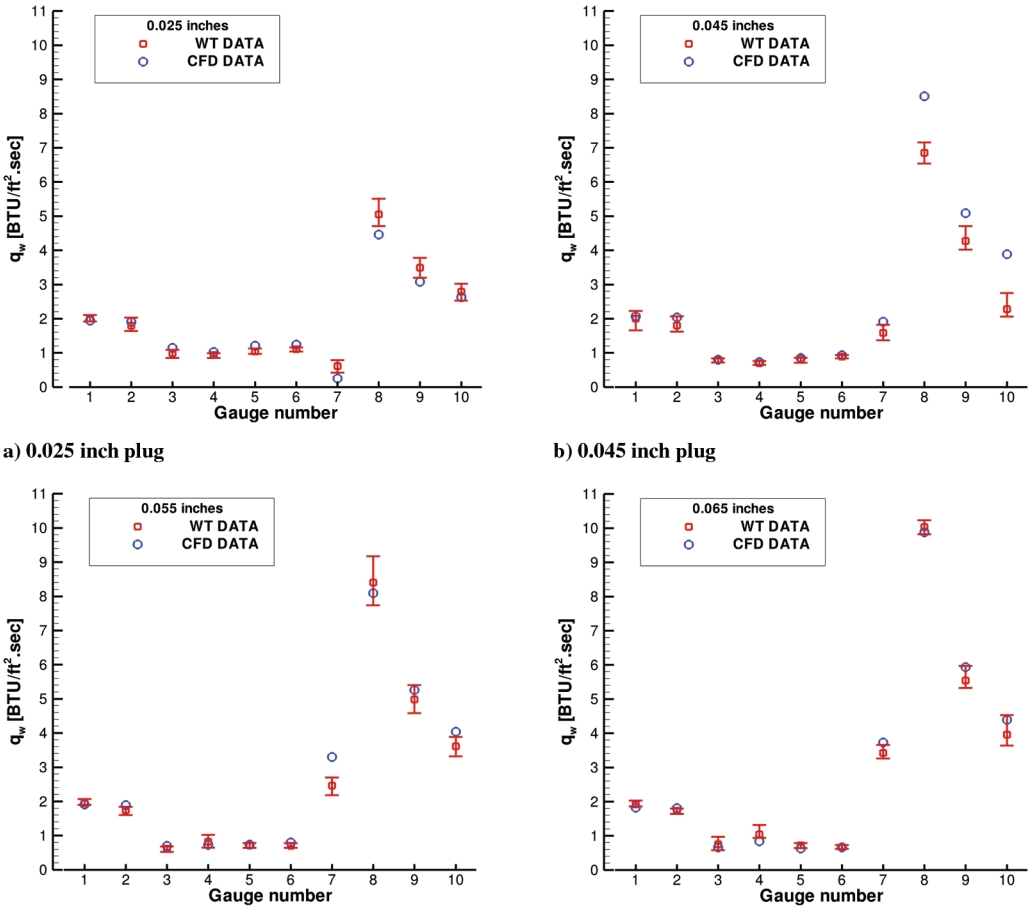

a) 0.025 inch plug

b) 0.045 inch plug

c) 0.055 inch plug

d) 0.065 inch plug

Fig. 10 WT and CFD data comparison at the vicinity of the plug lip.

conditions. This is obtained by calculating the peak heating rate at the lip of the plug, q_η, and the heat flux on the smooth surface without a plug at a location that would represent the base of the plug if it were present, $q_{\text{base}|_{\text{no plug}}}$ (see Fig. 11); that is,

$$\text{HA} = \frac{q_\eta}{q_{\text{base}|_{\text{no plug}}}} \tag{2}$$

The measured peak heating distance above the surface is shown schematically in Fig. 11 and tabulated in Table 4 for different plug heights. For the WT models, η is the location of the highest measured gauge.

Developing a Curve Fit

To obtain heat fluxes at the base of the plugs and on the smooth surface, q_{base}, simulations are performed on smooth WT swept-cylinder geometries. The peak heating rates are calculated from the gauge 8 locations (see Fig. 7). These data are shown in Fig. 12, in

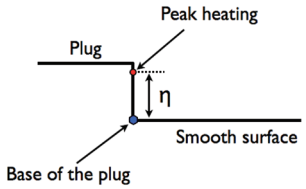

Fig. 11 Schematic illustration for heating-augmentation calculation [Eq. (2)].

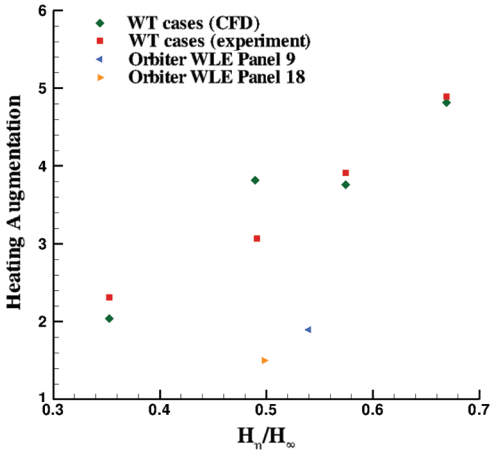

Fig. 12 First attempt to scale WT to flight data.

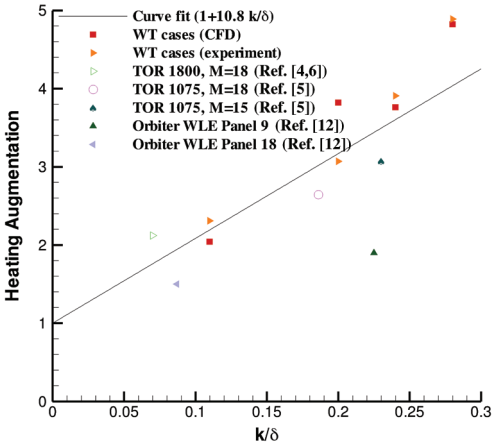

Fig. 13 Heating augmentation based on k/δ parameter, which does not fit the data well.

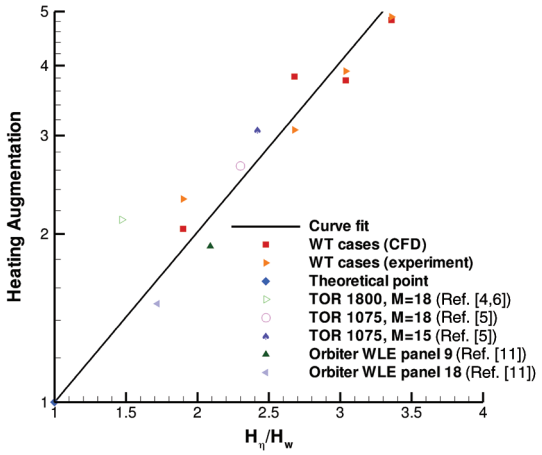

Fig. 14 Proposed heating-augmentation parameter for short hypersonic protuberances.

which the x axis is the ratio of peak heating to freestream enthalpy: H_η/H_∞. Heating augmentation on the Space Shuttle Orbiter WLE panels 9 and 18 (see [11]) are also computed and shown in this figure. The flight data show that a different correlation parameter is needed to correctly scale WT data (cold wall) to flight data (radiative equilibrium). It should be noted here that no conclusive explanation could be drawn as to why the comparison between CFD and experiment is higher for the enthalpy ratio: $H_\eta/H_\infty = 0.5$. This difference will be diminished, however, as a different correlation parameter is employed. LAURA is used for all CFD points.

An attempt was also made to examine k/δ as a correlation parameter. This parameter was used by Hung and Patel [13], primarily for large k/δ. They showed a large uncertainty in heating augmentation associated with this parameter. Our collection of data, shown in Fig. 13, also show that k/δ does not correlate well with a wide range of conditions.

Examining the enthalpy profile, it was found that the enthalpy profiles of the WT and flight cases start from a different value on the surface, due to different wall enthalpy values. Therefore, a correlation parameter was chosen that is based on the wall enthalpy values to collapse the WT and the CFD flight data (i.e., H_η/H_w). This correlation parameter is used in Fig. 14, in which the data are presented in log-linear format. Additional CFD flight cases from [4,5] are also added in this plot. Protuberances to the boundary-layer (BL) thickness ratio k/δ for all of the presented cases are less than 0.3. It appears that all of the presented data points but one are clustered around a single line.

The heating augmentation for the case in which $H_\eta/H_w = 1$, which is 1, is also shown. This point is called the theoretical point in this figure. The data are curve-fitted by anchoring the data to the theoretical point, and the following correlation is obtained:

$$\text{HA} = 0.5e^{0.7H_\eta/H_w} \tag{3}$$

Applying the Curve Fit

The curve fit is only tested for small k/δ. To use the proposed heating-augmentation correlation, only a flowfield solution over an undisturbed shuttle geometry is needed. The following steps are then needed to estimate the heating augmentation:

1) Locate smooth-OML geometry that would represent the base of the protuberance if it were present (the base of the protuberance is also defined as the impingement point).

2) Obtain the wall enthalpy at the identified location, H_w, from the solution.

3) Determine the height above the surface that would represent the height of the protuberance.

4) Obtain the enthalpy at the identified protuberance lip location, H_η, from the undisturbed flowfield solution.

5) Calculate the enthalpy ratio H_η/H_w.

6) Use the proposed correlation equation (3) to estimate the heating augmentation.

Conclusions

Several CFD analyses are conducted and compared with WT results for a swept-cylinder model with a protruding rounded plug. It is shown that the CFD data are in very good agreement with measured WT data. Based on the CFD and WT data, a heating-augmentation correlation that is based on an enthalpy profile is proposed. The proposed equation is examined for several CFD flight cases with short protuberances, in which the protuberance-to-BL-thickness ratio is less than 0.3, and a good agreement is achieved. Accordingly, the proposed correlation parameter shows potential for further investigation and testing against more flight cases.

Acknowledgment

The work of the first author is funded by NASA Langley Research Center through contact number NNL06AC49T.

References

[1] "Columbia Accident Investigation Board Final Report," Vols. 1–4, htttp://caib.nasa.gov, Oct. 2003.

[2] Hung, F., and Patel, D., "Protuberance lnterference Heating in High-Speed Flow," AIAA Paper 84-1724, 1984.

[3] Lessard, V. R., "CFD-Predicted Tile Heating Bump Factors Due to Tile Overlay Repairs," NASA Langley Research Center, NASA CR2006-214509, Hampton, VA, 2006.

[4] Mazaheri, A. R., "CFD Analysis of Tile-Repair Augers for the Shuttle Orbiter Re-Entry Aeroheating," NASA Langley Research Center CR2007-214858, Hampton, VA, 2007.

[5] Mazaheri, A. R., "Computational Aerothermodynamic Analysis of the Space Shuttle Orbiter Tile Overlay Repair with Different Geometries," NASA Johnson Space Center, Aeroscience and Flight Mechanics Division, EG-SS-07-17, 2007.

[6] Mazaheri, A. R., and Wood, W. A., "Re-Entry Aeroheating Analysis of Tile-Repair Augers for the Shuttle Orbiter," AIAA Paper 2007-4148, 2007.

[7] White, T., and Tang, C., "CFD Support for CUBRC RCC Repair," Johnson Space Center, Aeroscience and Flight Mechanics Div., Rept. EG-SS-08-01, Houston, TX, 2007.

[8] Gnoffo, P. A., "An Upwind-Biased, Point-Implicit Relaxation Algorithm for Viscous, Compressible Perfect-Gas Flows," NASA TP2953, Feb. 1990.

[9] Gnoffo, P. A., Gupta, R. N., and Shinn, J. L., "Conservation Equations and Physical Models for Hypersonic Air Flows in Thermal and Chemical Nonequilibrium," NASA TP2867, Feb. 1989.

[10] "Post Test Report for the Aerothermal Wind Tunnel Verification Test OH-200 RCC Repair C/SiC Plug and NOAX Crack Repair Model Configurations (Model 204-O)," The Boeing Company, Rept. SE07HB008, Huntington Beach, CA, 2007.

[11] Mazaheri, A. R., "Computational Aerothermodynamic Analysis of Wing Leading Edge Plug Models with Comparison to Wind Tunnel Experiments," NASA Johnson Space Center, Aeroscience and Flight Mechanics Div., Rept. EG-SS-07-18, Houston, TX, 2007.

[12] Cassady, A. M., Bourland, G., King, R., Kegerise, M., Marichalar, J., Kirk, B. S., and Trevino, L., "MH-13 Space Shuttle Orbiter Aerothermodynamic Test Report," NASA TP214758, 2007.

[13] Hung, F., and Patel, D., "Protuberance Interference Heating in High-Speed Flow," AIAA Paper 84-1724, 1984.

G. Palmer
Associate Editor